This is a non-peer-reviewed preprint submitted to EarthArXiv.

Vehicle-Based Methane Detection, Attribution, and Quantification in the Upstream Oil and Gas Sector: Method Overview and Controlled Release Validation

Robyn N. C. Latimer[1,2*], Evelise Bourlon[1], Khalil El Hachem[1], Pylyp Buntov[1], Jacob V. Johnson[3], Chukwuemeka V. Nwokoye[3], and David Risk[1]

[1]Department of Earth and Environmental Sciences, St. Francis Xavier University, Antigonish, Canada, B2G 2W5

[2]Department of Engineering and Applied Sciences, Memorial University of Newfoundland, St. John's, Canada, A1B 1T5

[3]Eotrac Incorporated, Dartmouth, Canada, B3B 1S1

[*]Corresponding author: rlatimer@stfx.ca

Vehicle-Based Methane Detection, Attribution, and Quantification in the Upstream Oil and Gas Sector: Method Overview and Controlled Release Validation

Robyn N. C. Latimer[1,2], Evelise Bourlon[1], Khalil El Hachem[1], Pylyp Buntov[1], Jacob V. Johnson[3♦], Chukwuemeka V. Nwokoye[3], and David Risk[1]*

[1]Department of Earth and Environmental Sciences, St. Francis Xavier University, Antigonish, Canada, B2G 2W5

[2]Department of Engineering and Applied Sciences, Memorial University of Newfoundland, St. John's, Canada, A1B 1T5

[3]Eotrac Incorporated, Dartmouth, Canada, B3B 1S1

[*]Email: rlatimer@stfx.ca

♦J.V.J. Deceased on October 9th, 2025.

KEYWORDS: methane detection, vehicle-based measurement, oil and gas, emission quantification, source attribution, controlled release experiment.

1. Abstract

Vehicle-based measurement systems occupy an important niche in the multi-scale methane measurement landscape between component-level technologies (e.g. OGI) and aerial-based methods. Performance evaluations are often limited to one dimension (e.g. quantification), while methodological opacity limits interpretation and inter-comparisons between technologies. Here, we develop a vehicle-based measurement system and processing framework incorporating a novel weighted likelihood algorithm for automated source attribution. Using controlled release experiments at two dedicated testing facilities, we characterize system performance across three dimensions – detection, attribution, and quantification. The system achieved a 96.1 % true positive detection rate with no false positives and a 90% detection limit as low as 0.024 kg/h with repeat transects. Attribution accuracy was high at the source-group level, reaching 99.7 % in single-source releases and 86 % in multi-source scenarios. Quantification was unbiased for low-to-moderate complexity releases (2 source groups; slope=0.99, R^2=0.81) but overestimated under highly complex conditions (5 source groups; slope=1.45, R^2=0.91). These results provide a transparent performance benchmark, demonstrating that these systems are well-suited to survey the large populations of low-to-moderate complexity sites (e.g. single wells and batteries), as a screening layer in LDAR applications and to quantify the low-end of emission distributions in inventories, reducing reliance on generic emission factors.

2. Introduction

Methane (CH_4), the primary component of natural gas, is a potent greenhouse gas with a 100-year global warming potential 27-30 times that of CO_2 [1]. The oil and gas (O&G) sector accounts for an estimated 44% of anthropogenic CH_4 emissions in Canada and 20% globally [2,3] and has been identified as a key sector for CH_4 emission reduction [4]. Jurisdictions including Canada, the United States (US), and the European Union have implemented regulations targeting CH_4 emissions from this sector [5–8]. These regulations mandate leak detection and repair (LDAR) programs under which regular site-level emission screening is conducted to identify and repair fugitive emission sources.

The growing interest in characterizing and reducing CH_4 emissions has driven the rapid development of CH_4 measurement technologies for two primary applications: targeted monitoring and mitigation (e.g. LDAR) and emission inventory development. Emerging regulatory programs have accelerated this trend by providing pathways for the use of alternative CH_4 measurement technologies beyond traditional optical gas imaging (OGI) surveys in LDAR programs [5,9]. These technologies include remote sensing methods (satellite, aerial, and drone) and ground-based approaches (vehicle-mounted, handheld, and stationary monitors). Fundamental trade-offs exist among these technologies in terms of spatial and temporal coverage, attribution granularity, cost, ease of deployment, detection sensitivity, and quantification accuracy. However, because of their different advantages and capabilities, there is a growing consensus that multi-scale measurements are essential for characterizing the overall CH_4 emission landscape [10–12].

Vehicle-based measurement systems occupy an important niche in this multi-scale measurement framework. Typically consisting of a vehicle equipped with a CH_4 analyzer, GPS, and meteorological sensors, these systems offer spatial coverage and detection sensitivity that fall

between component-level OGI surveys and larger-scale aerial measurements [13–15]. Here, we focus on fully mobile approaches that detect and quantify emissions during downwind transects, rather than methods that rely on extended measurements at fixed downwind locations (e.g., OTM-33A). Such vehicle-based systems have been used extensively to characterize CH_4 emissions from oil and gas production sites [16–20], urban environments and natural gas distribution networks [21–24], biogas facilities [25], and landfills [26]. In upstream O&G applications, emission rates are most commonly estimated using atmospheric concentration measurements coupled with atmospheric dispersion modelling in an inversion framework, although Lidar and tracer-based techniques have also been used [27].

To date, research on vehicle-based systems has largely focused on emission quantification, with comparatively less attention given to detection sensitivity and source localization. Localization approaches have varied widely across studies, including manual attribution [16,17,20], automated nearest-upwind-source algorithms whose reliability has not yet been evaluated [18,19], triangulation across multiple site visits under varying wind conditions [21], and optimization-based methods that, despite evaluating potential source locations within a defined boundary, exhibited localization errors of ~30–40 m within a 40–50 m domain [28,29]. Peer-reviewed controlled release evaluations of both localization and detection performance for vehicle-based solutions remain scarce. Ravikumar et al. [14] reported promising results for several systems, while Ilonze et al. [30] observed poor localization and were unable to establish a 90% probability of detection threshold for the single vehicle-based system tested. Field-based estimates suggest detection limits below 0.5 kg/h based on theoretical minimum detectable CH_4 enhancements and dispersion modeling [16,19], while controlled release experiments report limits ranging from 0.096 to > 10 kg/h [14]. This variability is difficult to interpret because it reflects differences in instrumentation, methodology, and operating

conditions, while many approaches rely on proprietary methods that are not fully disclosed. As a result, reproducibility is limited and inter-study comparability is constrained, ultimately presenting a barrier to the adoption of this technology in LDAR and inventory development applications.

In this study, we aim to improve the understanding of the role that vehicle-based measurement systems can play within a multi-scale measurement framework through a detailed methods description and comprehensive analysis of system performance. We develop a vehicle-based measurement system and processing framework for automated CH_4 detection, source attribution, and quantification in the upstream O&G sector. Using data collected from controlled-release experiments at two dedicated testing facilities that simulate realistic single- and multi-source upstream O&G emission scenarios, we present the first comprehensive and transparent performance characterization of a vehicle-based measurement system across three dimensions—detection, attribution, and quantification—and compare its capabilities with those of other commonly used CH_4 measurement technologies. In doing so, we aim to establish a performance benchmark that informs the broader scientific and regulatory communities about the capabilities, limitations, and potential role of vehicle-based systems in LDAR programs and CH_4 inventory development.

3. Materials and Methods

3.1. Vehicle-based Measurement System

Figure 1. Rooftop-mounted vehicle-based measurement system.

We collected measurements using a compact and portable vehicle-mounted system (Figure 1). Mounted to any vehicle using standard roof racks, the system consists of a tunable diode laser spectrometer (TDLAS; Axetris LGD Compact-A CH_4) with a precision (1σ) of ~0.2 ppm, a GPS (GlobalSat), and a 2-D ultra-sonic anemometer (Gill WindUltra). Ambient air is drawn from above the vehicle into an enclosure containing the TDLAS sensor by an air pump operating at a flow rate of 0.6 LPM, where CH_4 concentrations are measured. Measurements of CH_4 concentration, wind speed, wind direction, and vehicle location (latitude and longitude) are recorded at 2 Hz using a micro controller (ESP32). An internal modem enables wireless data transmission and real-time

data viewing on any browser-enabled device. The system is powered by a 12 V lithium battery, providing up to 8 hours of continuous operation, and has a total weight of <10 kg (22 pounds). Inlet height depends on the height of the vehicle upon which it is mounted- in this study, it was approximately 3 m. These measurements form the inputs to the processing framework described below.

3.2. Processing Framework

Our framework for processing vehicle-based CH_4 measurements operates on time series of atmospheric CH_4 concentration, wind speed, wind direction, and vehicle location (latitude and longitude) along the vehicle path, along with measurement height and the locations and heights of potential sources. It consists of four sequential steps: data preprocessing, CH_4 peak detection, source attribution, and quantification, each described in detail below.

3.2.1. Preprocessing

First, the raw measurement time series are cleaned, formatted, and prepared for subsequent analysis. This includes synchronizing measurements across instruments with different sampling frequencies onto a common timeline, interpolating missing values, and correcting raw measured wind speed and direction for vehicle motion. The CH_4 time series is shifted backward in time to account for sensor response time and transit time in tubing between the inlet and the gas analyzer.

Hourly observations of cloud cover, cloud ceiling height, and 10 m wind speed from the nearest airport are used to estimate discrete atmospheric stability classes [31]. In this approach, stability class is determined from wind speed and estimates of a net radiation index. This index depends on cloud cover, ceiling height, and insolation, which is estimated from solar altitude (a function of date, time, and location).

3.2.2. Peak detection

We analyze the CH_4 time series to identify elevated CH_4 values ("peaks"). First, we calculate a dynamic CH_4 baseline as an estimate of atmospheric background CH_4 concentrations using an iterative mean suppression method inspired by Liland [32] assuming that there are only CH_4 sources and no sinks, such that the lowest measured concentrations reflect background levels. We prepare the CH_4 signal by trimming leading and trailing NA values, thresholding the data to reduce the influence of large amplitude CH_4 peaks, mirroring the signal at both ends to avoid edge effects, and smoothing the resulting series. We then subsample the CH_4 data by taking the minimum value within fixed intervals to simplify the shape of the smoothed signal and increase speed.

We estimate the baseline iteratively on the prepared CH_4 time series by moving a window of exponentially decreasing sizes along the signal, calculating the mean value in each window and replacing values that exceed the mean with the mean. Each window is applied first to the right (time increasing direction) and then to the left to prevent directional bias.

We subtract the CH_4 baseline time series from the measured CH_4 time series to produce a time series of excess CH_4 (eCH_4), which is then used for peak detection. Peaks in the eCH_4 time series are identified using a spike detection algorithm described by Daniels et al. [33], which iterates through each observation and evaluates conditions that define the start, end, and validity of CH_4 peaks. The algorithm requires three input parameters which can be adjusted depending on the application and the sensitivity of the gas analyzer. Input parameter selection is discussed in more detail in Section S1 of the supplementary information (SI), and values used in this analysis are presented in Table S1. To minimize directional bias, we apply the algorithm in both the forward (time-increasing) and backward (time-decreasing) directions. We merge peaks detected during

both passes and assign sequential ID numbers from left to right. An example of the baseline calculation and spike detection algorithm outputs is shown in Figure S1.

3.2.3. Source attribution

Once the peaks in the eCH_4 time series have been identified, we attribute each peak to a known potential source location using a weighted likelihood algorithm that considers measured wind characteristics and the relative locations of the peak and source. We define the peak location as the latitude and longitude coordinates at which the maximum eCH_4 value of a peak was recorded. We define a metric called the total attribution weight (w_t) that characterizes the probability of a source to be the origin of the plume. For a given CH_4 peak, w_t (Eq. 1) is calculated as the product of a distance weight w_d and azimuth weight w_a for each source within a search radius d_{max} of the peak location.

$$w_t = w_d \times w_a \quad (1)$$

The distance weight depends on the distance from the source to the location of the measured peak. The x-axis is defined by the mean measured wind direction over a two-minute period. w_d decreases exponentially from 1 at an upwind distance (x) of 0 m to a minimum weight value w_{min} at a maximum distance d_{max} according to Eq. 2:

$$w_d = e^{\log\left(\frac{w_{min}}{d_{max}}\right)\left(x^2+y^2\right)^{0.5}} \qquad x \geq 0 \quad (2)$$

where y is the crosswind distance.

To consider the uncertainty of peak location, we also define an exponentially decreasing weight for negative upwind distances (i.e. downwind distances) to a much smaller downwind distance d_{back}, (Eq. 3).

$$w_d = e^{\log\left(\frac{w_{min}}{d_{max}}\right)\left(\left(x\frac{d_{max}}{d_{back}}\right)^2+y^2\right)^{0.5}} \qquad x < 0 \quad (3)$$

The azimuth weight (Eq. 4) depends on the azimuth of the source with the wind direction relative to the peak location and is represented by a scaled Gaussian function that covers a triangular area.

$$w_a = e^{\frac{-y^2}{2((x+ d_{back}) \sin(\sigma)^2)}} \quad x > -d_{back} \tag{4}$$

where σ , the standard deviation of the Gaussian function, is taken to be the standard deviation of the measured wind direction over a two-minute period. Figure S2 shows the distance, azimuth and total weights as a function of upwind and crosswind distance. Intuitively, the highest weights are assigned to sources that are directly upwind and close to the peak location.

3.2.4. Source Grouping

This vehicle-based method relies on downwind transect-based measurements of emitting sources. When individual equipment is co-located on a site, attribution of measured emissions at the source (equipment) level introduces additional uncertainty. In this framework, we group adjacent equipment into source groups. Depending on the use case, grouping can be done manually through visual inspection of source locations or automatically using hierarchical cluster analysis. The appropriate grouping radius depends on measurement distance: for on-pad measurements like those performed in this study, we group sources within a 10 m radius, while for more distant off-pad measurements, grouping distances of 45 m or more may be appropriate. Attribution weights are calculated for each individual source and each eCH_4 peak is attributed to the group containing the source with the highest individual attribution weight.

3.2.5. Quantification

An emission rate is estimated for each attributed CH_4 peak through comparison of measured eCH_4 values to those modelled with a Gaussian Plume Dispersion Model. This model is frequently employed to describe time-averaged atmospheric dispersion of non-reactive pollutants and

assumes the dispersion of these pollutants follows a normal distribution in the vertical (z) and crosswind (y) directions. It assumes steady-state, uniform wind conditions and treats the source as a continuous point emitter. The equation can be obtained as the stationary solution to the atmospheric diffusion equation [34]. For CH_4, total reflection of the plume off the ground is assumed, resulting in the following equation (Eq. 5) for modelled eCH_4 concentration at a point (x,y,z), where x is the along-wind distance from the source, y is the crosswind distance, and z is the height above ground, for an emitting source at height h:

$$eCH_{4,model}(x,y,z) = \frac{Q}{2\pi\sigma_y(x)\sigma_z(x)u} e^{\frac{-y^2}{2\sigma_y^2}} \left[e^{\frac{-(z-h)^2}{2\sigma_z^2(x)}} + e^{\frac{-(z+h)^2}{2\sigma_z^2(x)}} \right] \quad (5)$$

where Q is the emission rate of the source at point (0,0,h), u is the mean horizontal wind speed, and $\sigma_y(x)$ and $\sigma_z(x)$ are the horizontal and vertical dispersion coefficients, respectively, which depend on atmospheric stability and the downwind distance from the source. We calculate these dispersion coefficients according to parameterizations for rural environments [35]. For each attributed CH_4 peak, we determine wind direction using the geographic coordinates of the source and the peak, assuming the peak maximum occurs on the plume centerline directly downwind of the source. This is consistent with prior studies which have demonstrated that this assumption produces more accurate emission rate estimates than using measured wind directly [17,25,28,36], however it is a conservative assumption that could result in underestimation of emission rates if the true plume centerline was not transected. Following the same studies, modeled eCH_4 concentrations are calculated with Eq. 5 for each point in the measured CH_4 peak using a reference emission rate (Q_{ref}) of 1 g/s. The modeled and measured eCH_4 values are integrated (or summed) over the crosswind distance y, and the emission rate is estimated using Eq. 6.

$$Q_{est} = \frac{\sum eCH_{4,meas}}{\sum eCH_{4,model}} \times Q_{ref} \quad (6)$$

When quantifying emissions for a source group, we calculate individual emission rates for each source using its specific location and height and report the mean rate across the group. For sources sampled across multiple transects, we use the mean emission rate across transects, which has been shown to converge toward the true release rate, while the median tends to result in more pronounced underestimation [25,36]. If multiple source-groups on a site are tagged as emitting during a measurement event, the group-level rates are summed to obtain the site-level emission rate.

3.3. Controlled Release Experiments

Data from two controlled release experiments were used to evaluate the detection, attribution, and quantification performance of the vehicle-based CH_4 measurement system and processing framework. The measurements were conducted by Eotrac Incorporated (Eotrac) and provided for detailed analysis.

3.3.1. Measurement Protocol

Eotrac's standard work practice is five driven loops or "transects" around the periphery of the site, hereafter referred to as a "measurement event", at driving speeds between 5 to 10 km/h. In both controlled release experiments, Eotrac was informed of potential source locations; however, specific release locations and flow rates were kept blind during testing. Data was therefore collected in a way that is representative of upstream O&G field deployments, in which potential source locations on site are known, but the precise locations and rates are not.

3.3.2. Carbon Management Canada

Controlled release testing was conducted at the Carbon Management Canada (CMC) test facility at their Newel County field research station near Brooks, Alberta over five days from March 24 to 28, 2025. With five possible source locations divided into two source groups (Fig. 2, left), the site

configuration during these tests simulated real-world emission sources such as tanks, separator buildings, and well-pad equipment representative of a production site of low to moderate complexity. Release heights ranged from 0 to 5 m, and release rates ranged from 0.025 to 3.564 kg CH_4/h, with 74% of releases concentrated below 0.25 kg/h as shown in Figure 3 (left). In total, 97 measurement events were performed across five days, with events dominated by single-source releases (88%), followed by multi-source releases (8%), and no-source releases (4%).

3.3.3. Methane Emissions Technology Evaluation Center

Controlled release testing was conducted at the Methane Emissions Technology Evaluation Center (METEC) in Fort Collins, Colorado over three days from April 28 to 30, 2025. Releases followed the ADED 2.0 blind controlled testing protocol [37],which aims to simulate realistic multi-source emission scenarios representative of normal baseline operational emissions, periodic maintenance, and equipment failures. The portion of the site used for this experiment contained 24 potential source locations divided into five source groups (Fig. 2, right), including tanks, separators, and well pads, ranging in height from 1 to 5 m. Total site-level release rates ranged from 0.343 to 16.443 kg CH_4/h, with a cluster around 7 kg/h (Fig. 3, right). In total, 62 measurement events were performed, two of which were no-release, with the rest performed during multi-source releases with a mean of 4.5 emitting source groups per measurement event. With the large number of source groups and multi-source emission scenarios, this is representative of a highly complex O&G production site.

Figure 2. Map of the CMC (left) and METEC (right) controlled release facilities used in these experiments, showing individual source locations (blue circles), source groups (green outline), and full site (orange outline).

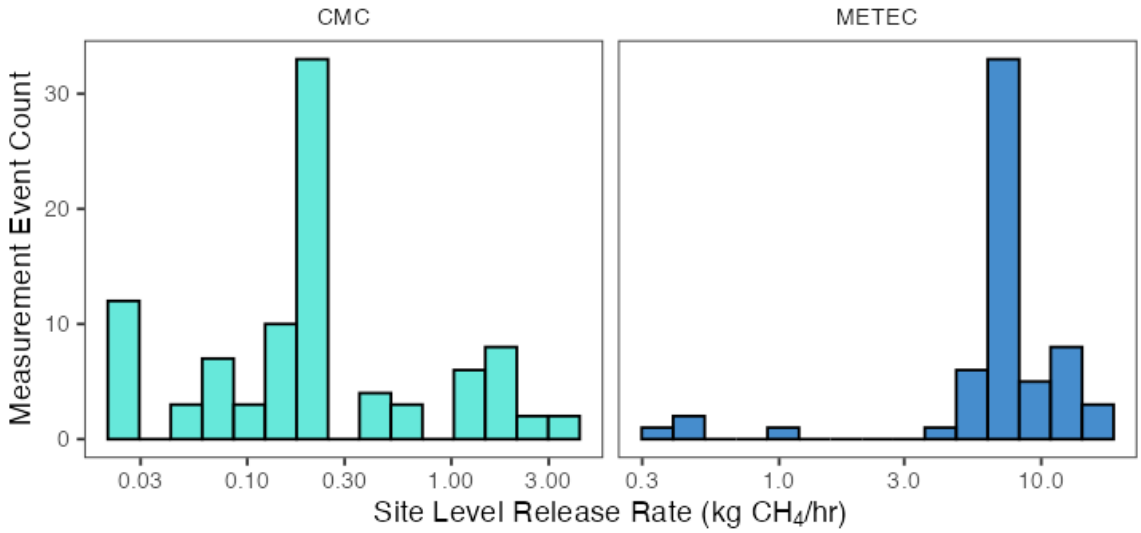

Figure 3. Distribution of site-level release rates across measurement events for the CMC (left) and METEC (right) controlled release experiments.

3.4. Analysis Methods

While measurements during the controlled-release experiments were conducted in a blinded fashion, the analysis presented here was performed after release rates and locations were unblinded

and provided by Eotrac, to facilitate evaluation of method performance. The processing framework used here differs slightly from that used by Eotrac, which may contribute to differences between our results and those reported in their controlled release white paper [38]. Data from both experiments were included in all analyses, except for the probability of detection (POD) analysis, which only used data collected during single-source release scenarios. The performance characterization presented here is specific to the hardware, processing framework, and measurement protocol applied in this study.

3.4.1. Detection Classifications

We evaluated overall detection performance at the measurement event level using all available controlled release data. A positive detection occurs if an eCH_4 peak is attributed to any equipment on site during a measurement event. We classified all measurement events (n=161) into four detection categories: true positive (TP), false positive (FP), true negative (TN), and false negative (FN) detections.

For a measurement event with a non-zero release rate, detection outcomes were classified as either TP, when emissions are present and a detection is reported, or FN, when emissions are present but no detection is reported. The fractions of each outcome were calculated using Eq. 7 and 8:

$$TP\ fraction = \frac{N_{TP}}{N_{TP} + N_{FN}} \quad (7)$$

$$FN\ fraction = \frac{N_{FN}}{N_{TP} + N_{FN}} \quad (8)$$

For a measurement event with a release rate of zero, outcomes were classified as either FP, when a detection is reported despite no emissions being present, or TN, when no detection is reported, calculated using Eq. 9 and 10:

$$FP\ fraction = \frac{N_{FP}}{N_{FP} + N_{TN}} \quad (9)$$

$$TN\ fraction = \frac{N_{TN}}{N_{FP} + N_{TN}} \quad (10)$$

These metrics represent the average detection performance across the range of conditions tested during the controlled release experiments, including release rates, source and site configurations, and meteorological conditions.

3.4.2. Evaluating Probability of Detection (POD)

We used individual transect-level data from single-source releases (n=428) to investigate factors impacting POD. Detection outcomes for each transect were classified by a binary detection variable (yes/no). Through a binary logistic regression, we explored factors influencing detection probability, including emission rate, source-sensor distance and height offset, and meteorological conditions. Emission rate was the dominant predictor, increasing the odds of detection by several orders of magnitude and substantially exceeding the effects of other predictors. Detection probability decreased with increasing distance and height offset, reflecting plume dilution and reduced plume intersection, and increased under more stable atmospheric conditions. However, limited coverage of these variables in the dataset limits our ability to fully evaluate their effects. Given the strong influence of emission rate, subsequent analysis focuses on the relationship between POD and emission rate, representing average detection performance across the sampling geometries and meteorological conditions encountered during the controlled release experiments.

We modeled the relationship between probability of detection (POD) and emission rate using an exponential function (Eq. 11), which ensures a POD of zero at an emission rate (x) of zero, and can represent the skewed nature of the response variable.

$$POD = 1 - e^{-a*x^b} \quad (11)$$

The curve fitting parameters (a and b) were estimated using a binary generalized linear model with a complementary log-log link function, using detection (yes/no) as the response variable and emission rate as the predictor. The input data consisted of single-transect measurements (one loop around the site). We characterized uncertainty via bootstrapping (1000 samples), where transects were sampled with replacement at each release rate magnitude, preserving the number of observations per rate. POD was calculated as the median of the bootstrapped distribution, with 95 % confidence interval defined by the 2.5 and 97.5 percentiles.

For multi-transect measurements, a positive detection occurs if there is a positive detection on any single transect. We calculated the multi-transect POD as a function of single-transect POD (POD_1) using Eq. 12:

$$POD_n = 1 - (1 - POD_1)^n \quad (12)$$

Detection limits corresponding to 50% and 90% POD and their 95% confidence intervals were calculated by inverting the fitted models and taking the median and 2.5 and 97.5 percentiles across the bootstrap distributions.

To contextualize the detection performance of this method relative to other technologies, we compiled lower detection limits from controlled release studies published since 2019. Studies were identified through Google Scholar searches targeting controlled release tests of OGI, handheld, stationary, vehicle, drone, aerial, and satellite technologies. Studies were selected based on relevance and availability of quantitative detection limit data. Detection limit ranges for each technology and corresponding references are provided in Table S2.

3.4.3. Attribution

We evaluated attribution performance for single- and multi-source release scenarios using the CMC and METEC controlled release data, respectively. For CMC single-source releases, there

was one true source and five potential source locations, divided into two source groups (Fig. 2, left). We assessed attribution accuracy as the percentage of CH_4 peaks correctly attributed at the source level, group level, and facility level (entire site). For METEC multi-source releases, up to five source groups were emitting simultaneously, and we assessed attribution accuracy as the percentage of emitting and non-emitting source groups correctly and incorrectly identified as emitting across all measurement events.

3.4.4. Quantification

We evaluated the quantification performance of the measurement system and processing framework by comparing estimated site-level emission rates to the true release rates. We excluded select CH_4 peaks from the analysis when they fell outside the "operational envelope" of the method, including peaks detected during stationary periods or very low driving speeds (<3 km/h), and peaks for which the ratio of horizontal source distance to the relative source-inlet vertical offset was less than 8:1. This reflects the physical limitations of measuring emissions from a tall source, and the need for adequate distance for the plume to disperse downward toward the inlet. Additionally, a source group had to be tagged on at least two transects to be included in quantification, increasing confidence in both attribution and emission rate estimates. After applying these criteria, we retained 72 of 89 CMC measurement events with detected emissions, while all METEC events were included, although the same restrictions were applied to individual peaks. We plotted true versus estimated site-level emission rates for each measurement event and performed a linear regression through the origin. Systematic bias in the method was evaluated via the slope of the best-fit line, where a slope near 1 indicates minimal bias, while R^2 captures the overall strength of the relationship between true and estimated rates. The fraction of emission

377 estimates within a factor of 2 (-50 to +100% error) and a factor of 3 (-67 to +200% error) of the
378 true release rate was also calculated.

379 As an example of regulatory LDAR applications in Canada, we defined emission rate bins by
380 order of magnitude (0-1, 1-10, 10-100 kg/h) to reflect the different repair timelines prescribed for
381 leaks of different magnitudes under Canada's amended oil and gas CH_4 regulations [7].We evaluated
382 the ability of this method to correctly triage site-level emission rates by the proportion of emission
383 rates correctly classified by magnitude bin.

384 **3.4.5. Site-level Emission Rate Uncertainty**

385 For each measurement event, we estimated site-level emission rate uncertainty using a
386 bootstrapping approach. For each iteration (n=1000), we resampled emission rate estimates with
387 replacement within each source group and calculated the mean emission rate across resampled
388 estimates. We summed source group means to produce a site-level total emission rate. This process
389 was repeated 1000 times per measurement event to generate empirical distributions of site-level
390 total emission rates, from which bootstrapped-derived 95% confidence intervals (2.5th and 97.5th
391 percentiles) were calculated. Only source groups with two or more emission rate estimates were
392 included. Relative uncertainty for each measurement event was calculated using Eq. 13:

393 $$Relative\ Uncertainty = \frac{(CI_{97.5} - CI_{2.5})/2}{\bar{Q}_{site}} \times 100 \quad (13)$$

394 Mean relative uncertainty was then calculated across all measurement events.

4. Results and Discussion

4.1. Detection Rate and Probability of Detection

Based on the combined results from the two controlled release experiments, the vehicle-based measurement system had a true positive detection rate of 96.1% across all measurement events (Figure 4). Out of the six events in which emissions were present but not detected (false negative), all six were at release rates < 1 kg/h, with 4/6 at the lowest emission rate tested (0.024 kg/h), and the remaining two from incomplete measurement events in which the measurement event only partially overlapped with the release timing, and consequently fewer than five transects were performed. The system exhibited a false positive rate of 0%, meaning emissions were only detected when they were truly present.

The detection sensitivity improves substantially with the number of measurement transects, as shown by POD curves as a function of the emission rate for 1-5 transects (Figure 5, left). For a single measurement transect, we estimated a 90% POD and 95% CI of 0.388 (0.291, 0.535) kg/h. This drops by a factor of three to 0.117 (0.093, 0.147) kg/h for two transects, continuing to drop with additional transects, reaching 0.024 (0.014, 0.036) kg/h for five transects, with marginal gains per additional transect beyond three (Figure 5, right).

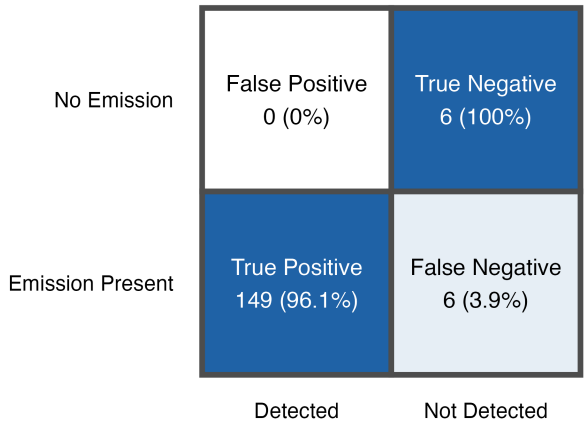

411

412 **Figure 4.** Confusion matrix of detection performance at the measurement-event level across both
413 controlled release experiments.

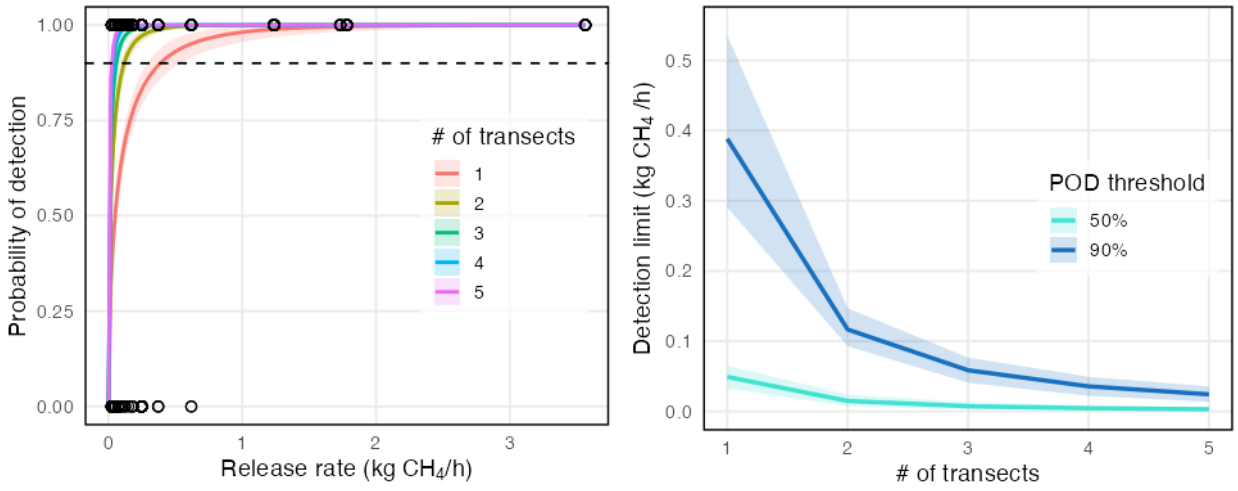

414

415 **Figure 5.** (Left) Probability of Detection curves as a function of release rate for 1-5 measurement
416 transects. (Right) Detection limit (kg CH4/h) as a function of the number of measurement transects
417 at 50% (light blue) and 90% (dark blue) probability of detection thresholds, with shaded regions
418 representing 95 % confidence interval.

419 The detection sensitivities reported here represent average performance across the conditions
420 encountered during the controlled release experiments for the measurement system tested. As the

CH_4 sensor used in this system has a relatively low measurement precision of ~0.2 ppm (1σ), detection sensitivity is expected to increase for more sensitive CH_4 sensors with which smaller perturbations in the CH_4 time series could be detected. Furthermore, as discussed in Section 2.3, detection performance is expected to vary with additional parameters identified in our binary logistic regression, including source-to-sensor distance and height offset, and atmospheric stability. While the release conditions are representative of typical on-site measurements of an O&G site, further investigation is needed to characterize the impact of these parameters on detection performance across a wider range of measurement conditions.

A key finding of this work is that detection sensitivity can be tuned by adjusting the number of measurement transects, rather than depending solely on refinements to the measurement system itself, e.g. increasing sensor precision. This illustrates a trade-off between sensor quality and measurement effort that can be leveraged to meet target detection thresholds. High detection sensitivities are achievable with a low-cost, lower-precision sensor than the research-grade analyzers (e.g., cavity ring-down or off-axis integrated cavity output spectroscopy instruments) typically employed in vehicle-based measurement studies, provided sufficient transects are performed. Based on the POD analysis, we recommend a minimum of three transects per measurement event, with up to five where detection of very low-emission sources is a priority.

Compared to other CH_4 detection technologies, including OGI and advanced handheld detection methods, this vehicle-based approach achieves comparable or superior detection performance with a lower detection limit well below the detection requirements for alternative technologies outlined in LDAR regulations [5,7,9]. Figure 6 illustrates the range of lower detection limits (90% POD detection thresholds when available) of CH_4 detection technologies from recent controlled release literature[13–15,30,39–45]. Specific detection limit ranges and references for each technology are listed

in Table S2. Ilonze et al.[30] reported 90% POD limits ranging from 0.06 to 1.32 kg/h for handheld OGI and from 0.04 to 1.15 kg/h for advanced handheld solutions, while Zimmerle et al. [15] reported 90% POD for OGI of 0.12 and 1.59 kg/h for surveyors with high and low experience, respectively. In contrast to OGI, the vehicle-based method is not expected to exhibit dependence on operator skill, provided simple driving instructions can be followed. There are, however, other potential limitations to applying this method, including site layouts that do not permit complete driven loops around the site. While detection performance was high across the range of emission heights tested here, previous studies have highlighted that truck-based detection performance may degrade for tall sources (e.g. tanks) compared to other equipment types [46].

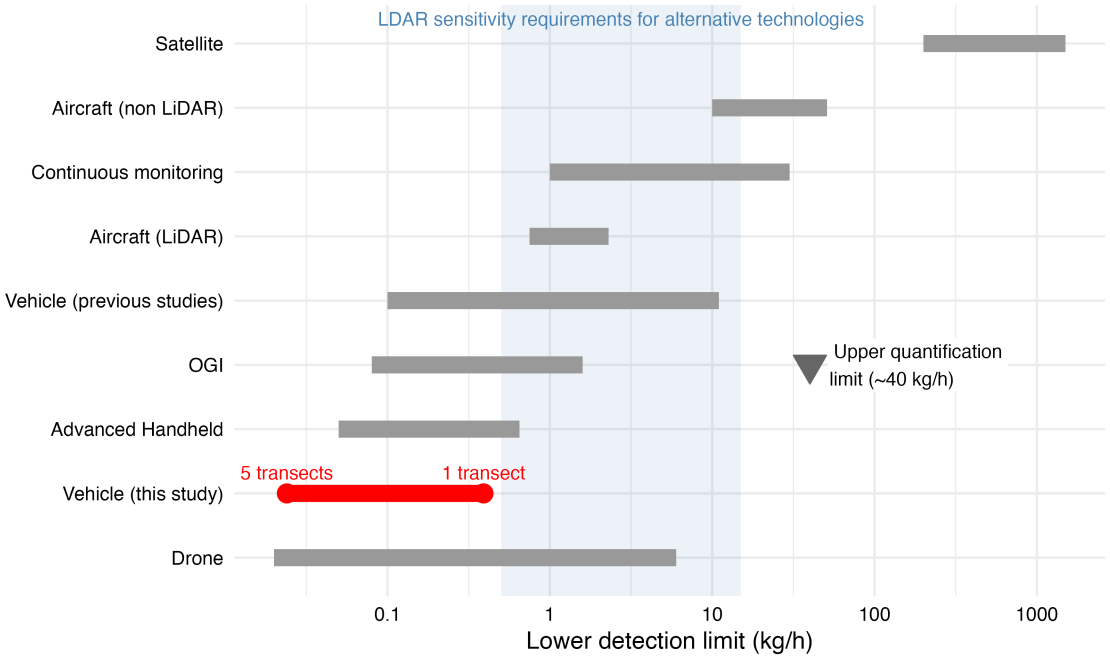

Figure 6. Comparison of CH_4 lower detection limit ranges across measurement technologies for other technologies (grey bars) and the vehicle-based method tested in this study (red bar). Detection limits represent 90% POD thresholds unless otherwise noted (Table S2). Ranges are derived from published literature. The shaded blue region represents the range of detection sensitivity requirements for use of alternative technology in LDAR programs; more sensitive

detection limits can result in reduced screening frequency requirements. The upper quantification limit for quantitative OGI (QOGI) technology is also shown (grey triangle).

4.2. Attribution Performance in Single- and Multi-Source Releases

In single-source release experiments, attribution accuracy was 100% at the site level, 99.7% at the group level, and 49% at the source level. These results indicate very strong performance in identifying the emitting source group, while highlighting challenges in pinpointing the precise within-group source. This limitation is expected for downwind mobile measurements, where uncertainty in the peak location combined with wind variability and plume turbulence make it difficult to resolve exact leak locations, and is consistent with findings from Ilonze et al. [30], who reported lower localization performance at the source (equipment) level for mobile solutions (vehicle and drone) relative to handheld technologies. For this reason, we opt to attribute peaks at the group level rather than the source level.

For the multi-source controlled release experiments conducted at METEC, attribution performance was assessed at the group level by determining whether emitting and non-emitting groups were correctly identified. Across all measurement events, 86% (n=238) of the 277 emitting groups were correctly tagged as emitting, and 15% (n=2) of the 13 non-emitting groups were incorrectly tagged as emitting. While attribution performance decreases slightly under complex multi-source release scenarios relative to single-source releases, the results demonstrate a strong performance in identifying emitting groups and a low false positive rate.

Overall, these results indicate that the measurement system is well-suited for identifying emission locations at the sub-facility scale, even in complex emission scenarios. This level of attribution granularity is sufficient for inventory applications, in which emission rates are typically reported at the facility scale. Furthermore, given the rapid site-level screening time (< 10 minutes),

this approach could be a valuable complement to more intensive LDAR survey techniques, enabling rapid triage and prioritization of component-level follow-up inspections.

4.3. Site-level Quantification Performance

Quantification performance varied significantly with release complexity. For low-to-moderate complexity release scenarios (1-2 emitting source groups), quantification performance was unbiased with a regression slope of 0.992 and R^2= 0.81 (Fig. 7, left). For high-complexity release scenarios (mean 4.5 simultaneous emitting source groups), estimated site-level emission rates were systematically higher than true release rates, with a regression slope of 1.45 and R^2=0.91 (Fig. 7, right). This overestimation of 45% is consistent with challenges in attributing emissions in an environment with multiple co-located source groups emitting simultaneously. In these scenarios, plume overlap between adjacent sources can increase the likelihood that emissions from one source are partially attributed to a neighbouring source, inflating total site-level emissions. The high R^2 value suggests that the method reliably captures relative differences in site-level emission rates despite these challenges with overestimation.

Overall, we find that 78% of emission estimates are within a factor of 2 error (-50 % to +100%) and 95% are within a factor of 3 error (-67% to +200%). Quantification error tends to be larger for small release magnitudes (see Figure S3), particularly below 1 kg/h. Across all individual measurement events, quantification error ranges from -50.4% to 347.5% (2.5^{th} to 97.5^{th} percentile), however when emission rates below 1 kg/h are excluded, this range narrows to -39.7% to 170.2%. Figure S4 shows uncertainty for each site-level emission estimate represented by error bars, derived via bootstrapping of individual emission estimates. Mean relative uncertainty across all measurement events was 40%, comparable to uncertainties reported for other CH_4 monitoring solutions [27,43].

These results are within a reasonable range of other vehicle-based quantification approaches, which have reported factor-of-two performance ranging from roughly 18–92% depending on the study and technology [14,27–29]. More broadly, the factor-of-two performance of 78% demonstrated here exceeds that of several other commonly used CH_4 quantification technologies. Factor-of-two performance ranging from 25-46% has been reported for QOGI [27,47] between 36-40 % for drone-based methods, between 50-78% for continuous monitors, and 33% for hi-flow samplers [27]. Our individual error range (95% CI) for rates above 1 kg/h (-39.7% to 170.2%) is comparable to that of Bridger Gas Mapping LiDAR (-58.5% to 129.4%, calculated from Bell et al. [48] SI), generally considered among the most accurate quantification technologies available but requiring greater logistical effort and cost.

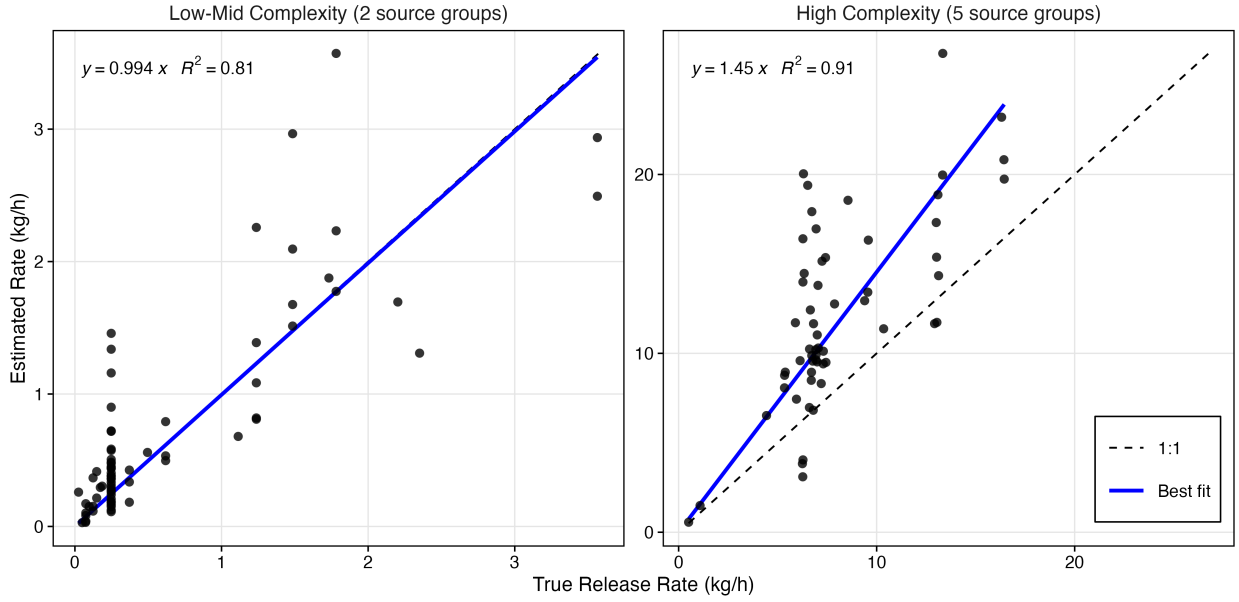

Figure 7. Estimated vs true site-level emission rates during the CMC experiments (left), representative of a low-to-moderate complexity site, and the METEC experiments (right), representative of a high complexity site. Linear regression line through the origin is shown in blue, and the 1:1 line is represented by the dashed line.

To our knowledge, this is the first study evaluating the quantification performance of this type of vehicle-based measurement system in release scenarios of varying complexity, as previous studies using this approach have focused exclusively on single-source release scenarios [25,28,29,36]. Our results highlight that complex multi-source scenarios introduce quantification challenges that are not present with a single source, but that the method reliably captures relative differences in site-level emission magnitudes as reflected in the high R^2 of 0.91. Future work should focus on refining methods for robust separation of overlapping plumes, to avoid double-counting emissions from co-located sources.

4.4. LDAR and Inventory Applications

We now examine how the system performance evaluated above translates to the two primary applications motivating this work: LDAR programs and emission inventory development. Categorization accuracy into Canada's regulatory LDAR repair threshold bins was high in the low-mid complexity release scenario at 94% (51/54) correct classification in the 0-1 kg/h bin and 83% (15/18) in the 1-10 kg/h bin (Table 1). In high complexity scenarios, classification accuracy was 100% in the 0-1 kg/h (1/1) and 10-100 kg/h (12/12) bins but dropped to 49% (22/45) for the 1-10 kg/h bin, largely due to the overestimation bias observed at complex release sites. With a mean true release rate of 6.7 kg/h in this bin, the systematic 45% overestimation shifted many estimates across the 10 kg/h threshold into the next regulatory bin. Notably, all misclassifications were off by only one bin, and most (26/29) were assigned to the higher bin rather than the lower, suggesting a conservative bias from a regulatory perspective.

Table 1. Summary of quantification and categorization performance of the vehicle-based measurement system.

Site Type	Magnitude bin (kg/h)	Num. meas. events	Mean release rate (kg/h)	MAE (kg/h)	MAPE	% correctly categorized
Low-Mid Complexity (CMC)	0-1	54	0.24	0.19	100%	94%
	1-10	18	1.78	0.58	34%	83%
High Complexity (METEC)	0-1	1	0.51	0.04	8%	100%
	1-10	45	6.71	4.60	69%	49%
	10-100	12	13.70	4.34	31%	100%

Results are divided by site complexity and emission rate magnitude bin. MAE= mean absolute error; MAPE= mean absolute percentage error. "% correctly categorized" reflects the proportion of total emission rate estimates that fell within the correct magnitude bin.

Although quantification performance degrades at high-complexity sites, this limitation should be considered in the context of LDAR requirements for the O&G site population. Under the amended Canadian oil and gas CH_4 regulations[7], survey requirements include comprehensive inspections between once per year to once per quarter for active sites, in addition to an annual third-party inspection and screening inspections multiple times per year at all sites. The regulation estimates approximately 447800 sites in Canada will be affected, of which active and inactive unplugged well sites together account for 412200 sites, or roughly 92% of the total site population. These well sites, along with facilities such as single-well batteries and small compressor stations, represent the types of low-to-moderate complexity sites where this method is expected to perform with minimal quantification bias.

Recent studies in Canada have found that OGI-based surveys miss a significant portion of total site-level emissions compared to aerial-based methods [12,49], highlighting critical gaps in LDAR programs that rely primarily on OGI measurements and emphasizing the need for multi-scale measurement approaches to capture the full emissions picture. In addition to demonstrating

561 comparable or greater detection sensitivity and superior quantification performance than OGI,
562 vehicle-based surveys offer several practical advantages that could address these gaps. At less than
563 10 minutes per site, vehicle-based surveys are significantly faster than OGI, where site-level
564 survey durations can range from 1-2 hours for satellite well pads to several days for large
565 facilities[50], enabling broad coverage of the large population of sites required under regulations.
566 The speed and scalability of vehicle-based surveys make them well-suited as a rapid-screening
567 layer, flagging sites and source groups for targeted OGI follow-up and directing those resources
568 where they are most needed. Operator-induced performance variability is also low compared to
569 OGI [15], and unlike aerial surveys in which the quality of modeled wind speed data from third-party
570 databases is a major contributor to uncertainty, the vehicle-based method measures wind
571 continuously and locally near the point of emission, which is important in complex environments.
572 Limitations include challenges in pinpointing individual leaking components, as well as
573 constraints common to ground-based methods more broadly: site-access constraints, such as
574 obstructions to full transects around a site, and unfavourable plume geometries arising from tall
575 sources measured at close range. In certain cases, tall and highly complex sites may therefore be
576 better suited to aerial survey methods. Taken together, these advantages and constraints suggest
577 that vehicle-based surveys could serve as a valuable complement to, rather than replacement for,
578 component-level OGI surveys and aerial approaches.

579 Beyond LDAR applications, vehicle-based measurement methods could help to fill a persistent
580 gap in emission inventory development by increasing the number of low-level emitters that are
581 directly measured. Emissions from oil and gas are well-documented to follow a heavy-tailed
582 distribution, where a relatively small number of large emitters contribute disproportionately to
583 total emissions [18,51–53]. However, low-level emitters remain an important and often under

584 considered component of the inventory picture. Conrad et al.[54] estimated that 24% of provincial
585 CH_4 emissions in Alberta originated from sources below the detection limit of the Bridger Gas
586 Mapping LiDAR, with their bottom-up inventory relying primarily on equipment counts, emission
587 factors, and OGI data rather than direct measurement. Similarly, Williams et al.[53] estimated that
588 30% of CH_4 emissions from O&G sites across the contiguous United States originate from sources
589 emitting less than 10 kg/h. Ravikumar et al.[55] demonstrated that a detection limit of 0.1 kg/h is
590 sufficient to maximize detected emissions from the O&G sector during periodic leak surveys, a
591 threshold well within the sensitivity demonstrated here. The performance demonstrated in this
592 study, particularly the 90% POD threshold as low as 0.024 kg/h and the near-unbiased
593 quantification performance at low-to-moderate complexity sites, suggests that the vehicle-based
594 method is well-suited to characterize the lower end of the emission distribution that aerial and
595 satellite methods are likely to miss, with considerably less time and effort than methods of
596 comparable detection sensitivity such as QOGI, thereby reducing reliance on generic emission
597 factors and limited component-level data.

598 Future work should focus on characterizing the influence of measurement distance and source
599 height on detection performance, validating quantification performance at higher emission
600 magnitudes, and developing reliable methods for the separation of overlapping plumes from
601 closely co-located sources in order to address overestimation at high complexity sites. Together,
602 these advances would further establish vehicle-based measurements as a high-performance and
603 practical complement to existing CH_4 monitoring approaches.

5. REFERENCES

(1) Forster, P.; Storelvmo, T.; Armour, K.; Collins, W.; Dufresne, J.-L.; Frame, D.; Lunt, D. J.; Mauritsen, T.; Palmer, T.; Watanabe, M.; Zhang, H. The Earth's Energy Budget, Climate Feedbacks, and Climate Sensitivity. In *Climate Change 2021 – The Physical Science Basis: Working Group I Contribution to the Sixth Assessment Report of the Intergovernmental Panel on Climate Change*; Cambridge University Press: 923 Cambridge, United Kingdom and New York, NY, USA, 2021; pp 923–1054. https://doi.org/10.1017/9781009157896.

(2) Environment and Climate Change Canada (ECCC). National Inventory Report 1990-2024: Greenhouse Gas Sources and Sinks in Canada, 2026.

(3) Saunois, M.; Martinez, A.; Poulter, B.; Zhang, Z.; Raymond, P. A.; Regnier, P.; Canadell, J. G.; Jackson, R. B.; Patra, P. K.; Bousquet, P.; Ciais, P.; Dlugokencky, E. J.; Lan, X.; Allen, G. H.; Bastviken, D.; Beerling, D. J.; Belikov, D. A.; Blake, D. R.; Castaldi, S.; Crippa, M.; Deemer, B. R.; Dennison, F.; Etiope, G.; Gedney, N.; Höglund-Isaksson, L.; Holgerson, M. A.; Hopcroft, P. O.; Hugelius, G.; Ito, A.; Jain, A. K.; Janardanan, R.; Johnson, M. S.; Kleinen, T.; Krummel, P. B.; Lauerwald, R.; Li, T.; Liu, X.; McDonald, K. C.; Melton, J. R.; Mühle, J.; Müller, J.; Murguia-Flores, F.; Niwa, Y.; Noce, S.; Pan, S.; Parker, R. J.; Peng, C.; Ramonet, M.; Riley, W. J.; Rocher-Ros, G.; Rosentreter, J. A.; Sasakawa, M.; Segers, A.; Smith, S. J.; Stanley, E. H.; Thanwerdas, J.; Tian, H.; Tsuruta, A.; Tubiello, F. N.; Weber, T. S.; van der Werf, G. R.; Worthy, D. E. J.; Xi, Y.; Yoshida, Y.; Zhang, W.; Zheng, B.; Zhu, Q.; Zhu, Q.; Zhuang, Q. Global Methane Budget 2000–2020. *Earth Syst. Sci. Data* **2025**, *17* (5), 1873–1958. https://doi.org/10.5194/essd-17-1873-2025.

(4) Ocko, I. B.; Sun, T.; Shindell, D.; Oppenheimer, M.; Hristov, A. N.; Pacala, S. W.; Mauzerall, D. L.; Xu, Y.; Hamburg, S. P. Acting Rapidly to Deploy Readily Available Methane

Mitigation Measures by Sector Can Immediately Slow Global Warming. *Environ. Res. Lett.* **2021**, *16* (5), 054042. https://doi.org/10.1088/1748-9326/abf9c8.

(5) Environmental Protection Agency (EPA). *Standards of Performance for New, Reconstructed, and Modified Sources and Emissions Guidelines for Existing Sources: Oil and Natural Gas Sector Climate Review*; 89; 40 CFR Part 60; RIN 2060-AV16; 2024. https://www.federalregister.gov/documents/2024/03/08/2024-00366/standards-of-performance-for-new-reconstructed-and-modified-sources-and-emissions-guidelines-for (accessed 2026-04-28).

(6) Government of Canada. *Regulations Respecting Reduction in the Release of Methane and Certain Volatile Organic Compounds (Upstream Oil and Gas Sector)*; Volume 152; SOR/2018-66; Canada Gazette, Part 2, 2018.

(7) Government of Canada. *Regulations Amending the Regulations Respecting Reduction in the Release of Methane and Certain Volatile Organic Compounds (Upstream Oil and Gas Sector)*; Volume 159; SOR/2025-280; Canada Gazette, Part 2, 2025. https://gazette.gc.ca/rp-pr/p2/2025/2025-12-31/html/sor-dors280-eng.html (accessed 2026-04-28).

(8) European Parliament, Council of the European Union. *Regulation (EU) 2024/1787 of the European Parliament and of the Council on the Reduction of Methane Emissions in the Energy Sector and Amending Regulation (EU) 2019/942*; 2024; Vol. OJ L, 2024/1787. https://eur-lex.europa.eu/legal-content/EN/ALL/?uri=CELEX:32024R1787.

(9) Alberta Energy Regulator (AER). Directive 060: Upstream Petroleum Industry Flaring, Incinerating, and Venting, 2025. https://www.aer.ca/regulations-and-compliance-enforcement/rules-and-regulations/directives/directive-060.

(10) Daniels, W. S.; Wang, J. L.; Ravikumar, A. P.; Harrison, M.; Roman-White, S. A.; George, F. C.; Hammerling, D. M. Toward Multiscale Measurement-Informed Methane Inventories: Reconciling Bottom-Up Site-Level Inventories with Top-Down Measurements Using Continuous Monitoring Systems. *Environ. Sci. Technol.* **2023**, *57* (32), 11823–11833. https://doi.org/10.1021/acs.est.3c01121.

(11) Fox, T. A.; Barchyn, T. E.; Risk, D.; Ravikumar, A. P.; Hugenholtz, C. H. A Review of Close-Range and Screening Technologies for Mitigating Fugitive Methane Emissions in Upstream Oil and Gas. *Environ. Res. Lett.* **2019**, *14* (5), 053002. https://doi.org/10.1088/1748-9326/ab0cc3.

(12) Wilde, S. E.; Tyner, D. R.; Johnson, M. R. The Efficacy of Methane Leak Detection and Repair (LDAR) Programs in Practice. *ACS EST Air* **2025**, *2* (11), 2527–2536. https://doi.org/10.1021/acsestair.5c00195.

(13) Conrad, B. M.; Tyner, D. R.; Johnson, M. R. Robust Probabilities of Detection and Quantification Uncertainty for Aerial Methane Detection: Examples for Three Airborne Technologies. *Remote Sens. Environ.* **2023**, *288*, 113499. https://doi.org/10.1016/j.rse.2023.113499.

(14) Ravikumar, A. P.; Sreedhara, S.; Wang, J.; Englander, J.; Roda-Stuart, D.; Bell, C.; Zimmerle, D.; Lyon, D.; Mogstad, I.; Ratner, B.; Brandt, A. R. Single-Blind Inter-Comparison of Methane Detection Technologies – Results from the Stanford/EDF Mobile Monitoring Challenge. *Elem. Sci. Anthr.* **2019**, *7*, 37. https://doi.org/10.1525/elementa.373.

(15) Zimmerle, D.; Vaughn, T.; Bell, C.; Bennett, K.; Deshmukh, P.; Thoma, E. Detection Limits of Optical Gas Imaging for Natural Gas Leak Detection in Realistic Controlled Conditions. *Environ. Sci. Technol.* **2020**, *54* (18), 11506–11514. https://doi.org/10.1021/acs.est.0c01285.

(16) Caulton, D. R.; Lu, J. M.; Lane, H. M.; Buchholz, B.; Fitts, J. P.; Golston, L. M.; Guo, X.; Li, Q.; McSpiritt, J.; Pan, D.; Wendt, L.; Bou-Zeid, E.; Zondlo, M. A. Importance of Superemitter Natural Gas Well Pads in the Marcellus Shale. *Environ. Sci. Technol.* **2019**, *53* (9), 4747–4754. https://doi.org/10.1021/acs.est.8b06965.

(17) Korbeń, P.; Jagoda, P.; Maazallahi, H.; Kammerer, J.; Nęcki, J. M.; Wietzel, J. B.; Bartyzel, J.; Radovici, A.; Zavala-Araiza, D.; Röckmann, T.; Schmidt, M. Quantification of Methane Emission Rate from Oil and Gas Wells in Romania Using Ground-Based Measurement Techniques. *Elem. Sci. Anthr.* **2022**, *10* (1), 00070. https://doi.org/10.1525/elementa.2022.00070.

(18) MacKay, K.; Lavoie, M.; Bourlon, E.; Atherton, E.; O'Connell, E.; Baillie, J.; Fougère, C.; Risk, D. Methane Emissions from Upstream Oil and Gas Production in Canada Are Underestimated. *Sci. Rep.* **2021**, *11* (1), 8041. https://doi.org/10.1038/s41598-021-87610-3.

(19) O'Connell, E.; Risk, D.; Atherton, E.; Bourlon, E.; Fougère, C.; Baillie, J.; Lowry, D.; Johnson, J. Methane Emissions from Contrasting Production Regions within Alberta, Canada: Implications under Incoming Federal Methane Regulations. *Elem. Sci. Anthr.* **2019**, *7*, 3. https://doi.org/10.1525/elementa.341.

(20) Zhou, X.; Yoon, S.; Mara, S.; Falk, M.; Kuwayama, T.; Tran, T.; Cheadle, L.; Nyarady, J.; Croes, B.; Scheehle, E.; Herner, J. D.; Vijayan, A. Mobile Sampling of Methane Emissions from Natural Gas Well Pads in California. *Atmos. Environ.* **2021**, *244*, 117930. https://doi.org/10.1016/j.atmosenv.2020.117930.

(21) Ars, S.; Vogel, F.; Arrowsmith, C.; Heerah, S.; Knuckey, E.; Lavoie, J.; Lee, C.; Pak, N. M.; Phillips, J. L.; Wunch, D. Investigation of the Spatial Distribution of Methane Sources in the

691 Greater Toronto Area Using Mobile Gas Monitoring Systems. *Environ. Sci. Technol.* **2020**, *54*
692 (24), 15671–15679. https://doi.org/10.1021/acs.est.0c05386.

693 (22) Tettenborn, J.; Zavala-Araiza, D.; Stroeken, D.; Maazallahi, H.; Van Der Veen, C.; Hensen,
694 A.; Velzeboer, I.; Van Den Bulk, P.; Vogel, F.; Gillespie, L.; Ars, S.; France, J.; Lowry, D.; Fisher,
695 R.; Röckmann, T. Improving Consistency in Methane Emission Quantification from the Natural
696 Gas Distribution Systems across Measurement Devices. *Atmospheric Meas. Tech.* **2025**, *18* (14),
697 3569–3584. https://doi.org/10.5194/amt-18-3569-2025.

698 (23) Vogel, F.; Ars, S.; Wunch, D.; Lavoie, J.; Gillespie, L.; Maazallahi, H.; Röckmann, T.;
699 Nęcki, J.; Bartyzel, J.; Jagoda, P.; Lowry, D.; France, J.; Fernandez, J.; Bakkaloglu, S.; Fisher, R.;
700 Lanoiselle, M.; Chen, H.; Oudshoorn, M.; Yver-Kwok, C.; Defratyka, S.; Morgui, J. A.; Estruch,
701 C.; Curcoll, R.; Grossi, C.; Chen, J.; Dietrich, F.; Forstmaier, A.; Denier Van Der Gon, H. A. C.;
702 Dellaert, S. N. C.; Salo, J.; Corbu, M.; Iancu, S. S.; Tudor, A. S.; Scarlat, A. I.; Calcan, A. Ground-
703 Based Mobile Measurements to Track Urban Methane Emissions from Natural Gas in 12 Cities
704 across Eight Countries. *Environ. Sci. Technol.* **2024**, *58* (5), 2271–2281.
705 https://doi.org/10.1021/acs.est.3c03160.

706 (24) von Fischer, J. C.; Cooley, D.; Chamberlain, S.; Gaylord, A.; Griebenow, C. J.; Hamburg,
707 S. P.; Salo, J.; Schumacher, R.; Theobald, D.; Ham, J. Rapid, Vehicle-Based Identification of
708 Location and Magnitude of Urban Natural Gas Pipeline Leaks. *Environ. Sci. Technol.* **2017**, *51*
709 (7), 4091–4099. https://doi.org/10.1021/acs.est.6b06095.

710 (25) Wietzel, J. B.; Korben, P.; Hoheisel, A.; Schmidt, M. Best Practices and Uncertainties in
711 CH_4 Emission Quantification: Employing Mobile Measurements and Gaussian Plume Modelling
712 at a Biogas Plant. April 10, 2025. https://doi.org/10.5194/egusphere-2025-1344.

(26) Gillespie, L. D.; Ars, S.; Alkadri, S.; Urya, S.; Khoo, T.; Fraser, S.; Vogel, F.; Wunch, D. Estimating Methane Emissions from the Waste Sector in Southern Ontario Using Atmospheric Measurements. *J. Air Waste Manag. Assoc.* **2025**, *75* (2), 144–163. https://doi.org/10.1080/10962247.2024.2435340.

(27) Liu, Y.; Paris, J.-D.; Broquet, G.; Bescós Roy, V.; Meixus Fernandez, T.; Andersen, R.; Russu Berlanga, A.; Christensen, E.; Courtois, Y.; Dominok, S.; Dussenne, C.; Eckert, T.; Finlayson, A.; Fernández De La Fuente, A.; Gunn, C.; Hashmonay, R.; Grigoleto Hayashi, J.; Helmore, J.; Honsel, S.; Innocenti, F.; Irjala, M.; Log, T.; Lopez, C.; Cortés Martínez, F.; Martinez, J.; Massardier, A.; Nygaard, H. G.; Agregan Reboredo, P.; Rousset, E.; Scherello, A.; Ulbricht, M.; Weidmann, D.; Williams, O.; Yarrow, N.; Zarea, M.; Ziegler, R.; Sciare, J.; Vrekoussis, M.; Bousquet, P. Assessment of Current Methane Emission Quantification Techniques for Natural Gas Midstream Applications. *Atmospheric Meas. Tech.* **2024**, *17* (6), 1633–1649. https://doi.org/10.5194/amt-17-1633-2024.

(28) Kumar, P.; Broquet, G.; Yver-Kwok, C.; Laurent, O.; Gichuki, S.; Caldow, C.; Cropley, F.; Lauvaux, T.; Ramonet, M.; Berthe, G.; Martin, F.; Duclaux, O.; Juery, C.; Bouchet, C.; Ciais, P. Mobile Atmospheric Measurements and Local-Scale Inverse Estimation of the Location and Rates of Brief CH₄ and CO₂ Releases from Point Sources. *Atmospheric Meas. Tech.* **2021**, *14* (9), 5987–6003. https://doi.org/10.5194/amt-14-5987-2021.

(29) Kumar, P.; Broquet, G.; Caldow, C.; Laurent, O.; Gichuki, S.; Cropley, F.; Yver-Kwok, C.; Fontanier, B.; Lauvaux, T.; Ramonet, M.; Shah, A.; Berthe, G.; Martin, F.; Duclaux, O.; Juery, C.; Bouchet, C.; Pitt, J.; Ciais, P. Near-field Atmospheric Inversions for the Localization and

735 Quantification of Controlled Methane Releases Using Stationary and Mobile Measurements. *Q. J.*
736 *R. Meteorol. Soc.* **2022**, *148* (745), 1886–1912. https://doi.org/10.1002/qj.4283.

737 (30) Ilonze, C.; Day, R.; Emerson, E.; Duggan, A.; Brouwer, R.; Zimmerle, D. Performance
738 Evaluation of Survey Solutions in Detecting and Localizing Source-Level Emissions Using a
739 Single-Blind Controlled Testing Protocol. *Environ. Sci. Technol.* **2026**, *60* (1), 459–472.
740 https://doi.org/10.1021/acs.est.5c11814.

741 (31) Turner, D. B. A Diffusion Model for an Urban Area. *J. Appl. Meteorol.* **1964**, *3*, 83–91.
742 https://doi.org/10.1175/1520-0450(1964)003%3C0083:ADMFAU%3E2.0.CO;2.

743 (32) Liland, K. H. 4S Peak Filling – Baseline Estimation by Iterative Mean Suppression.
744 *MethodsX* **2015**, *2*, 135–140. https://doi.org/10.1016/j.mex.2015.02.009.

745 (33) Daniels, W. S.; Jia, M.; Hammerling, D. M. Detection, Localization, and Quantification of
746 Single-Source Methane Emissions on Oil and Gas Production Sites Using Point-in-Space
747 Continuous Monitoring Systems. *Elem Sci Anth* **2024**, *12* (1), 00110.
748 https://doi.org/10.1525/elementa.2023.00110.

749 (34) Seinfeld, J. H.; Pandis, S. N. *Atmospheric Chemistry and Physics: From Air Pollution to*
750 *Climate Change*, 1st ed.; New York Academy of Sciences Series; John Wiley & Sons,
751 Incorporated: Newark, 2016.

752 (35) Turner, D. B. Workbook of Atmospheric Dispersion Estimates, 1970.

753 (36) Caulton, D. R.; Li, Q.; Bou-Zeid, E.; Fitts, J. P.; Golston, L. M.; Pan, D.; Lu, J.; Lane, H.
754 M.; Buchholz, B.; Guo, X.; McSpiritt, J.; Wendt, L.; Zondlo, M. A. Quantifying Uncertainties
755 from Mobile-Laboratory-Derived Emissions of Well Pads Using Inverse Gaussian Methods.

Atmospheric Chem. Phys. **2018**, *18* (20), 15145–15168. https://doi.org/10.5194/acp-18-15145-2018.

(37) Methane Emission Technology Evaluation Center (METEC) and TotalEnergies Anomalies Detection Initiatives (TADI). Controlled Test Protocol, Emission Detection and Quantification Protocol (Version Number 1.0). **2025**.

(38) Eotrac Incorporated. *Characterizing the Performance of a Mobile Methane Detection Platform: Insights from Controlled Release Testing in Alberta*; Calgary, AB, Canada, 2025. https://www.eotrac.com/news/vehicle-mounted-methane-detection-whitepaper (accessed 2026-04-16).

(39) Bell, C.; Rutherford, J.; Brandt, A.; Sherwin, E.; Vaughn, T.; Zimmerle, D. Single-Blind Determination of Methane Detection Limits and Quantification Accuracy Using Aircraft-Based LiDAR. *Elem. Sci. Anthr.* **2022**, *10* (1), 00080. https://doi.org/10.1525/elementa.2022.00080.

(40) El Abbadi, S. H.; Chen, Z.; Burdeau, P. M.; Rutherford, J. S.; Chen, Y.; Zhang, Z.; Sherwin, E. D.; Brandt, A. R. Technological Maturity of Aircraft-Based Methane Sensing for Greenhouse Gas Mitigation. *Environ. Sci. Technol.* **2024**, *58* (22), 9591–9600. https://doi.org/10.1021/acs.est.4c02439.

(41) Bell, C.; Ilonze, C.; Duggan, A.; Zimmerle, D. Performance of Continuous Emission Monitoring Solutions under a Single-Blind Controlled Testing Protocol. *Environ. Sci. Technol.* **2023**, *57* (14), 5794–5805. https://doi.org/10.1021/acs.est.2c09235.

(42) Ilonze, C.; Emerson, E.; Duggan, A.; Zimmerle, D. Assessing the Progress of the Performance of Continuous Monitoring Solutions under a Single-Blind Controlled Testing

Protocol. *Environ. Sci. Technol.* **2024**, *58* (25), 10941–10955. https://doi.org/10.1021/acs.est.3c08511.

(43) McManemin, A.; Juéry, C.; Blandin, V.; France, J. L.; Burdeau, P.; Brandt, A. R. Controlled Release Testing of Commercially Available Methane Emission Measurement Technologies at the TADI Facility. *Atmospheric Meas. Tech.* **2026**, *19* (3), 923–934. https://doi.org/10.5194/amt-19-923-2026.

(44) Sherwin, E. D.; Rutherford, J. S.; Chen, Y.; Aminfard, S.; Kort, E. A.; Jackson, R. B.; Brandt, A. R. Single-Blind Validation of Space-Based Point-Source Detection and Quantification of Onshore Methane Emissions. *Sci. Rep.* **2023**, *13* (1), 3836. https://doi.org/10.1038/s41598-023-30761-2.

(45) Sherwin, E. D.; El Abbadi, S. H.; Burdeau, P. M.; Zhang, Z.; Chen, Z.; Rutherford, J. S.; Chen, Y.; Brandt, A. R. Single-Blind Test of Nine Methane-Sensing Satellite Systems from Three Continents. *Atmospheric Meas. Tech.* **2024**, *17* (2), 765–782. https://doi.org/10.5194/amt-17-765-2024.

(46) Singh, D.; Barlow, B.; Hugenholtz, C.; Funk, W.; Robinson, C.; Ravikumar, A. *Field Performance of New Methane Detection Technologies: Results from the Alberta Methane Field Challenge*; preprint; Oil, Gas, and Energy, 2021. https://doi.org/10.31223/X5GS46.

(47) Ilonze, C.; Wang, J. (Lyra); Ravikumar, A. P.; Zimmerle, D. Methane Quantification Performance of the Quantitative Optical Gas Imaging (QOGI) System Using Single-Blind Controlled Release Assessment. *Sensors* **2024**, *24* (13), 4044. https://doi.org/10.3390/s24134044.

(48) Bell, C.; Rutherford, J.; Brandt, A.; Sherwin, E.; Vaughn, T.; Zimmerle, D. Single-Blind Determination of Methane Detection Limits and Quantification Accuracy Using Aircraft-Based LiDAR. *Elem. Sci. Anthr.* **2022**, *10* (1), 00080. https://doi.org/10.1525/elementa.2022.00080.

(49) Tyner, D. R.; Johnson, M. R. Where the Methane Is—Insights from Novel Airborne LiDAR Measurements Combined with Ground Survey Data. *Environ. Sci. Technol.* **2021**, *55* (14), 9773–9783. https://doi.org/10.1021/acs.est.1c01572.

(50) Ravikumar, A. P.; Roda-Stuart, D.; Liu, R.; Bradley, A.; Bergerson, J.; Nie, Y.; Zhang, S.; Bi, X.; Brandt, A. R. Repeated Leak Detection and Repair Surveys Reduce Methane Emissions over Scale of Years. *Environ. Res. Lett.* **2020**, *15* (3), 034029. https://doi.org/10.1088/1748-9326/ab6ae1.

(51) Alvarez, R. A.; Zavala-Araiza, D.; Lyon, D. R.; Allen, D. T.; Barkley, Z. R.; Brandt, A. R.; Davis, K. J.; Herndon, S. C.; Jacob, D. J.; Karion, A.; Kort, E. A.; Lamb, B. K.; Lauvaux, T.; Maasakkers, J. D.; Marchese, A. J.; Omara, M.; Pacala, S. W.; Peischl, J.; Robinson, A. L.; Shepson, P. B.; Sweeney, C.; Townsend-Small, A.; Wofsy, S. C.; Hamburg, S. P. Assessment of Methane Emissions from the U.S. Oil and Gas Supply Chain. *Science* **2018**, eaar7204. https://doi.org/10.1126/science.aar7204.

(52) Brandt, A. R.; Heath, G. A.; Cooley, D. Methane Leaks from Natural Gas Systems Follow Extreme Distributions. *Environ. Sci. Technol.* **2016**, *50* (22), 12512–12520. https://doi.org/10.1021/acs.est.6b04303.

(53) Williams, J. P.; Omara, M.; Himmelberger, A.; Zavala-Araiza, D.; MacKay, K.; Benmergui, J.; Sargent, M.; Wofsy, S. C.; Hamburg, S. P.; Gautam, R. Small Emission Sources in Aggregate Disproportionately Account for a Large Majority of Total Methane Emissions from the

US Oil and Gas Sector. *Atmospheric Chem. Phys.* **2025**, *25* (3), 1513–1532. https://doi.org/10.5194/acp-25-1513-2025.

(54) Conrad, B. M.; Tyner, D. R.; Li, H. Z.; Xie, D.; Johnson, M. R. A Measurement-Based Upstream Oil and Gas Methane Inventory for Alberta, Canada Reveals Higher Emissions and Different Sources than Official Estimates. *Commun. Earth Environ.* **2023**, *4* (1), 416. https://doi.org/10.1038/s43247-023-01081-0.

(55) Ravikumar, A. P.; Wang, J.; McGuire, M.; Bell, C. S.; Zimmerle, D.; Brandt, A. R. "Good versus Good Enough?" Empirical Tests of Methane Leak Detection Sensitivity of a Commercial Infrared Camera. *Environ. Sci. Technol.* **2018**, *52* (4), 2368–2374. https://doi.org/10.1021/acs.est.7b04945.

Supplementary Materials

Vehicle-Based Methane Detection, Attribution, and Quantification in the Upstream Oil and Gas Sector: Method Overview and Controlled Release Validation

Robyn N.C. Latimer[1,2*], Evelise Bourlon[1], Khalil El Hachem[1], Pylyp Buntov[1], Jacob V. Johnson[3], Chukwuemeka V. Nwokoye[3], David Risk[1]

[1]Department of Earth and Environmental Sciences, St. Francis Xavier University, Antigonish, Canada, B2G 2W5

[2]Department of Engineering and Applied Sciences, Memorial University of Newfoundland, St. John's, Canada, A1B 1T5

[3]Eotrac Incorporated, Dartmouth, Canada, B3B 1S1

*Email: rlatimer@stfx.ca

S1 Input Parameter Selection for Spike Detection Algorithm

The spike detection algorithm described in Daniels et al. requires three input parameters:

1. **Going-up threshold (ppm):** a peak begins when the increase in consecutive concentration values exceeds this threshold.
2. **Return threshold (%):** a peak ends when the concentration value returns to this predefined percentage of the maximum peak value.
3. **Peak amplitude threshold (ppm):** a peak is retained if the maximum concentration value of the peak exceeds this threshold.

The selection of input parameters depends on the use-case scenario. As described by Daniels et al. (2024), the parameters were designed to balance each other out and therefore do not require precise tuning. For example, the going-up-threshold should be set to a value much lower than the peak amplitude threshold, to tag peaks that build more slowly. Any peak that fails to reach the peak amplitude threshold will be filtered out. Table S1 outlines the input parameters chosen for the Axetris gas analyzer. Figure S1 shows the result of the spike detection algorithm applied to the CH_4 timeseries.

An advantage to this algorithm is that it can be applied directly to raw instrument signals without requiring noise filtering, provided the peak amplitude threshold is set above the instrument noise level. Noise filtering can alter the max eCH_4 location and peak amplitude, two parameters that must be known as precisely as possible for our attribution and quantification steps.

873 **Table S2**. Input parameters for spike detection algorithm.

Input Parameter	**Value**
Going-up Threshold	0.05 ppm
Amplitude Threshold	0.5 ppm
Return Threshold	50 %

874

875

Figure S8. Timeseries of measured CH_4 concentration (black), calculated CH_4 baseline (red), CH_4 peaks (turquoise), and peak maxima (blue).

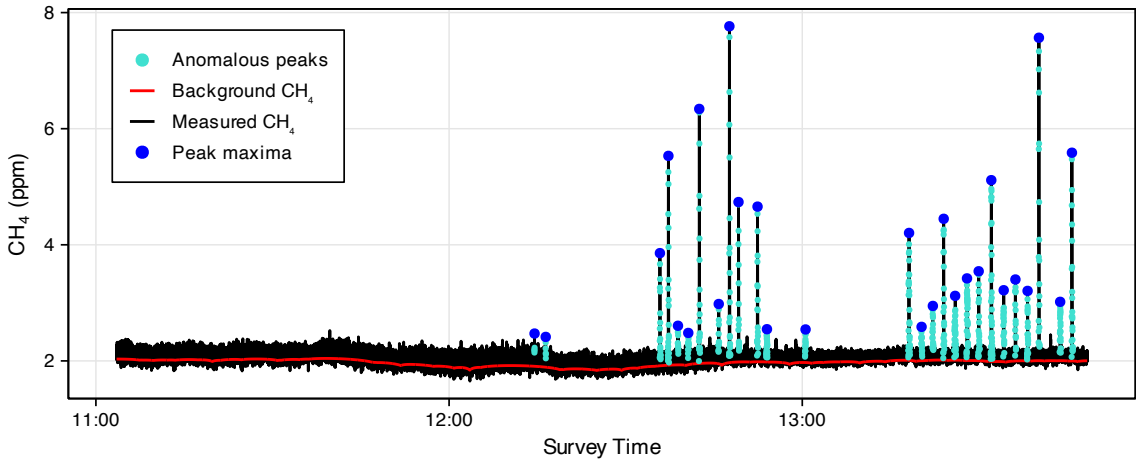

Figure S9. Attribution distance weight (a), azimuth weight (b) and total weight (c) as a function of upwind and crosswind distance

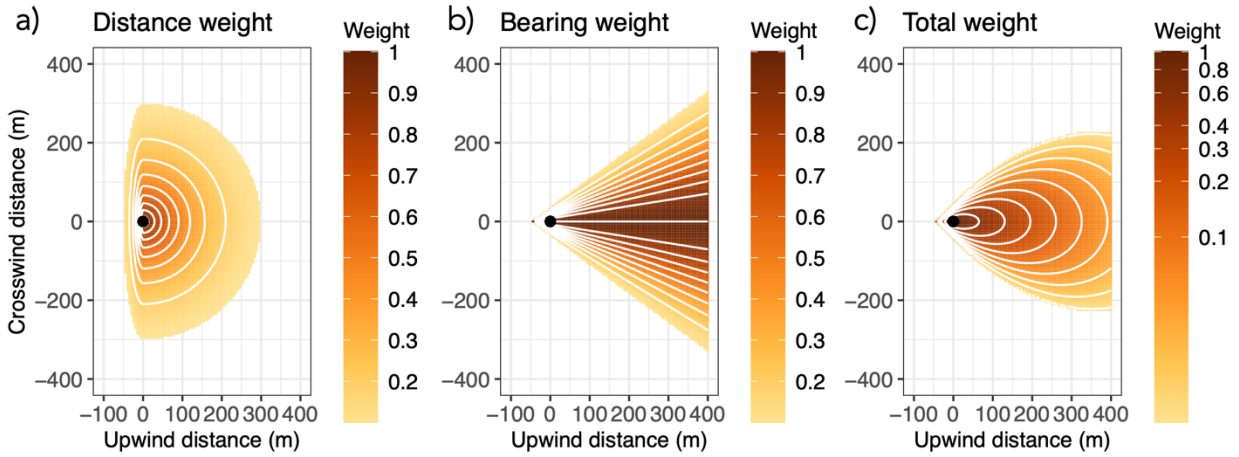

Table S3. Lower detection limit ranges and corresponding references for various CH_4 monitoring technologies. Detection limits correspond to 90% probability of detection thresholds unless otherwise noted.

Technology	Lower Detection Limit Range (kg/h)	References
OGI	0.06 to 1.593	Ilonze et al., 2026 Zimmerle et al., 2020
Advanced Handheld	0.04 to 0.65	Ilonze et al., 2026
Aircraft LiDAR	0.75 to 2.3	Bell et al., 2022[1] Conrad et al., 2023[1]
Aircraft (non-LiDAR)	10 to 51	Conrad et al., 2023[2] El Abbadi et al., 2024[3]
Continuous Monitoring	1 to 30	Bell et al., 2023 Ilonze et al., 2024 McManemin et al., 2026
Drone	0.02 to 6	McManemin et al., 2026 Ravikumar et al., 2019[4]
Vehicle (previous studies)	0.1 to 11	Ravikumar et al., 2019[4]
Satellite	200 to 1500	Sherwin et al., 2023, 2024[5]
Vehicle (this study)	0.024 to 0.39	This study

[1] At reference windspeed of 3 m/s and typical altitude of 152 m (Bell et al.) and 175 m (Conrad et al.)

[2] At reference windspeed of 3 m/s and typical altitude of 900 m for Kairos and 3000 m for AVIRIS-NG

[3] 90 % detection limit not reported, aircraft consistently quantified emissions above 10 kg/h

[4] Reports rates where POD is 100%

[5] Approximate detection limits

Figure S10. Percent quantification error by release magnitude bin.

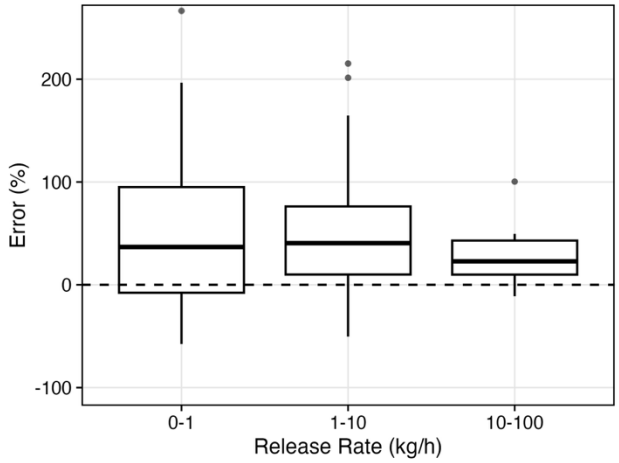

Figure S11. Estimated vs true site-level emission rates during the CMC experiments (left), representative of a low-to-moderate complexity site, and the METEC experiments (right), representative of a high complexity site. Linear regression line through the origin is shown in blue, and the 1:1 line is represented by the dashed line. Uncertainty for each site-level emission estimate represented by error bars, derived via bootstrapping of individual emission estimates.

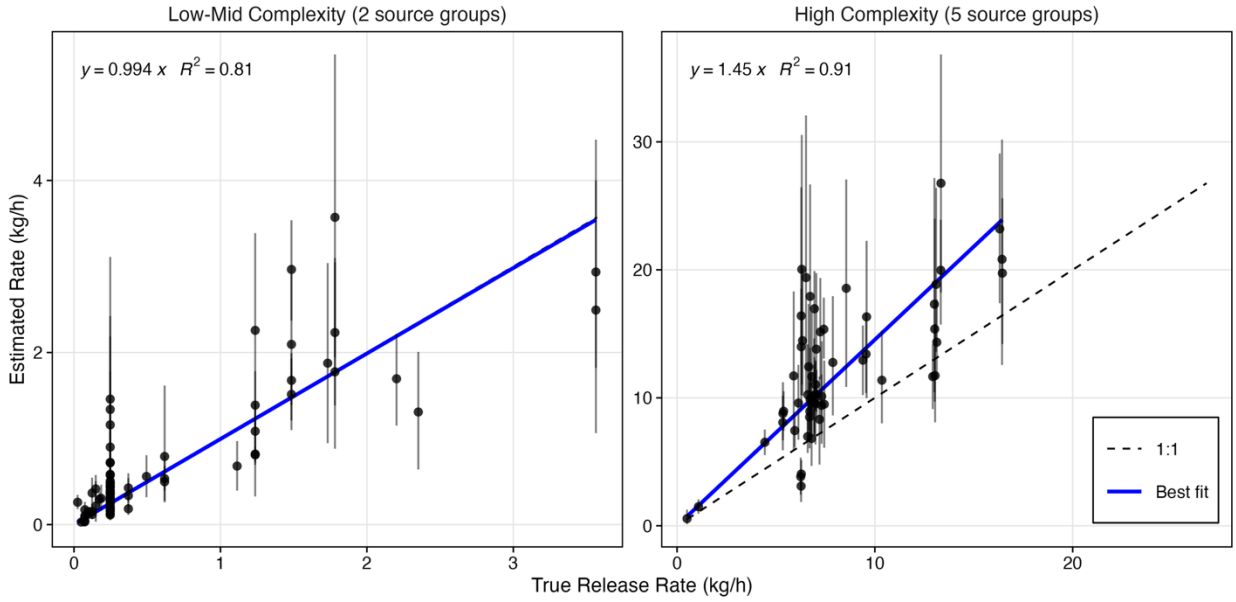

6. References

Bell, C., Ilonze, C., Duggan, A., & Zimmerle, D. (2023). Performance of Continuous Emission Monitoring Solutions under a Single-Blind Controlled Testing Protocol. *Environmental Science & Technology*, *57*(14), 5794–5805. https://doi.org/10.1021/acs.est.2c09235

Bell, C., Rutherford, J., Brandt, A., Sherwin, E., Vaughn, T., & Zimmerle, D. (2022). Single-blind determination of methane detection limits and quantification accuracy using aircraft-based LiDAR. *Elementa: Science of the Anthropocene*, *10*(1), 00080. https://doi.org/10.1525/elementa.2022.00080

Conrad, B. M., Tyner, D. R., & Johnson, M. R. (2023). Robust probabilities of detection and quantification uncertainty for aerial methane detection: Examples for three airborne technologies. *Remote Sensing of Environment*, *288*, 113499. https://doi.org/10.1016/j.rse.2023.113499

Daniels, W. S., Jia, M., & Hammerling, D. M. (2024). Detection, localization, and quantification of single-source methane emissions on oil and gas production sites using point-in-space continuous monitoring systems. *Elem Sci Anth*, *12*(1), 00110. https://doi.org/10.1525/elementa.2023.00110

El Abbadi, S. H., Chen, Z., Burdeau, P. M., Rutherford, J. S., Chen, Y., Zhang, Z., Sherwin, E. D., & Brandt, A. R. (2024). Technological Maturity of Aircraft-Based Methane Sensing for Greenhouse Gas Mitigation. *Environmental Science & Technology*, *58*(22), 9591–9600. https://doi.org/10.1021/acs.est.4c02439

Ilonze, C., Day, R., Emerson, E., Duggan, A., Brouwer, R., & Zimmerle, D. (2026). Performance Evaluation of Survey Solutions in Detecting and Localizing Source-Level Emissions Using

a Single-Blind Controlled Testing Protocol. *Environmental Science & Technology*, *60*(1), 459–472. https://doi.org/10.1021/acs.est.5c11814

Ilonze, C., Emerson, E., Duggan, A., & Zimmerle, D. (2024). Assessing the Progress of the Performance of Continuous Monitoring Solutions under a Single-Blind Controlled Testing Protocol. *Environmental Science & Technology*, *58*(25), 10941–10955. https://doi.org/10.1021/acs.est.3c08511

McManemin, A., Juéry, C., Blandin, V., France, J. L., Burdeau, P., & Brandt, A. R. (2026). Controlled release testing of commercially available methane emission measurement technologies at the TADI facility. *Atmospheric Measurement Techniques*, *19*(3), 923–934. https://doi.org/10.5194/amt-19-923-2026

Ravikumar, A. P., Sreedhara, S., Wang, J., Englander, J., Roda-Stuart, D., Bell, C., Zimmerle, D., Lyon, D., Mogstad, I., Ratner, B., & Brandt, A. R. (2019). Single-blind inter-comparison of methane detection technologies – results from the Stanford/EDF Mobile Monitoring Challenge. *Elementa: Science of the Anthropocene*, *7*, 37. https://doi.org/10.1525/elementa.373

Sherwin, E. D., El Abbadi, S. H., Burdeau, P. M., Zhang, Z., Chen, Z., Rutherford, J. S., Chen, Y., & Brandt, A. R. (2024). Single-blind test of nine methane-sensing satellite systems from three continents. *Atmospheric Measurement Techniques*, *17*(2), 765–782. https://doi.org/10.5194/amt-17-765-2024

Sherwin, E. D., Rutherford, J. S., Chen, Y., Aminfard, S., Kort, E. A., Jackson, R. B., & Brandt, A. R. (2023). Single-blind validation of space-based point-source detection and quantification of onshore methane emissions. *Scientific Reports*, *13*(1), 3836. https://doi.org/10.1038/s41598-023-30761-2

Zimmerle, D., Vaughn, T., Bell, C., Bennett, K., Deshmukh, P., & Thoma, E. (2020). Detection Limits of Optical Gas Imaging for Natural Gas Leak Detection in Realistic Controlled Conditions. *Environmental Science & Technology*, *54*(18), 11506–11514. https://doi.org/10.1021/acs.est.0c01285